

Understanding the critical instability in the climate of North Atlantic Region using Data Science

Alka Yadav¹, Sourish Das^{2,*}, Anirban Chakraborti^{1,3,*}, and Koyel Sur^{4,+}

¹Jawaharlal Nehru University, School of Computational and Integrative Sciences, New Delhi-110067, India.

²Chennai Mathematical Institute, Chennai-603103, India.

³BML Munjal University, School of Engineering and Technology, Gurugram-122413, India.

⁴Punjab Remote Sensing Centre, Ludhiana-141004, India.

*sourish@cmi.ac.in

*anirban.chakraborti@bmu.edu.in

ABSTRACT

A negative (or positive) value of the North Atlantic Oscillation (NAO) index, which measures the variability in sea-level atmospheric pressure, would imply increase (or decrease) in intense cold air outbreaks and the number of storms in the eastern parts of North America and Northern Europe. The NAO may be influenced by several climate factors. Using a data science approach, here we aim to study the complex dynamics that NAO has with the sea surface temperature (SST) and sea ice extent (SIE), and show that there exists a critical instability (through positive feedback loops) in the complex dynamics of the climate variables of melting Arctic SIE, rising SST, and NAO index. Our statistical machine learning approach shows that the melting SIE and increasing SST significantly affect the NAO, resulting in the changing weather pattern of the North Atlantic region. We also develop a Bayesian Granger-causal dynamic linear model to establish the relationship between the predictor and dependent variable. Our study indicates that there would be a critical instability with more frequent bouts of very cold climate in eastern North America and northern Europe than previously seen, marking a significant climate change.

Introduction

After the first industrial revolution, anthropogenic factors have primarily driven the complex dynamics of climatic elements on the earth¹, causing alarming changes and often critical instabilities (resulting from positive feedback loops) in the climate. We can see the indications of climate change in the different climate variables like sea surface temperature (SST), atmospheric pressure at sea level, Arctic sea ice extent (SIE), etc. Among other indicators, one of the popular indices that measures the variability of atmospheric pressure at sea level is the North Atlantic Oscillation (NAO)². In eastern North America and northern Europe, a negative value of NAO would be associated with increase in the number of storms and strong cold air outbreaks. However, a positive value of NAO would indicate fewer cold air outbreaks with decrease in the number of storms².

It has been known that there is a positive feedback loop between the high melting rate of the Arctic SIE³ and the rising SST. Oceans tend to absorb more heat over the years due to increased concentrations of greenhouse gases in the atmosphere. This aggravates global atmospheric circulation, directly influencing the SIE melting⁴. The melting SIE in turn would affect the rising SST and consequently the atmospheric pressure at sea level. Researchers have also highlighted the fact that atmospheric circulation along the trajectories influences NAO on a sub-seasonal timescale and lead to rapid melting of SIE^{5,6}. Several scientific research communities and international forums like Intergovernmental Panel for Climate Change (IPCC) have predicted a 50% decrease in SIE over the next 50 years^{7,8}. Therefore, NAO would have a significant role in rapid climate change because it acts as the prime source of ocean heat transport⁹. Castro-Diez *et al.*¹⁰ had explored the relationship between NAO and the temperature of southern Europe and brought out its sensitivity towards both phases of NAO. Warner *et al.*¹¹ had investigated whether or not the Arctic SIE is the physical driver of NAO variability. Several studies investigated the relations between NAO and SST at a *small regional scale* along the Atlantic Ocean^{10,12–19}. It was evident that the primary source of inter-annual variability within the atmospheric circulation pattern was NAO, and it was accountable for more than one-third of the variability in atmospheric pressure at sea level²⁰. However, the closed coupling factor between NAO and SST indicated cold SST during the positive NAO, and vice versa²¹. Parkinson²² had also explored the possible link between the melting of the SIE and the NAO index using satellite-based information. Koslowski²³ had earlier established that the accumulated ice volume negatively correlates with the NAO index over the Baltic sea. Further, Kwok²⁰ had also tried to establish patterns of variability in the ice motion that can be linked to the NAO index over the Arctic Sea and Barent Sea. It was also reported that there exists a negative impact of melting SIE at the Labrador Sea on the variability of the NAO²⁴. Bader *et al.*²⁵ had presented a review that examines the impacts of sea-ice loss and effects on the NAO. Caian *et al.*²⁶ presented a link between Arctic sea-ice surface

variability and the phases of the NAO during the winter. Tian and Fan²⁷ developed a new statistical forecast scheme using observed autumn SST and Eurasian snow cover to predict the winter NAO in the preceding autumn. Kolstad and Screen²⁸ used multiple climate models to discover the evidence of a non-stationary correlation between the sea ice at Barents-Kara during autumn and the winter NAO. Other than Parkinson²², almost all others^{20,23–26,28–30} were done for specific seas of the Arctic Ocean and only for the winter season. Most of the studies on SIE were based on computationally intensive climate models that restricted their areas of interest in specific regions of Arctic and North Atlantic regions.

In this study, our aim is to understand the complex dynamics (as shown in Figure 1) and critical instability (through positive feedback loops) among the climate variables of the melting SIE, rising SST, and NAO, using a very generic approach of statistical machine learning and over the *entire* North Atlantic region. This approach would be more general than the sophisticated climate forecast models²⁸. A major criticism of the statistical models has been that it was always assumed that the predictor’s relationship with the dependent variable did not change over time²⁸. Our study addresses this criticism by adopting a Bayesian Granger-causal dynamic linear model, inspired from earlier works^{31–33}, so that relationship between the predictor and the dependent variable is dynamically updated over time.

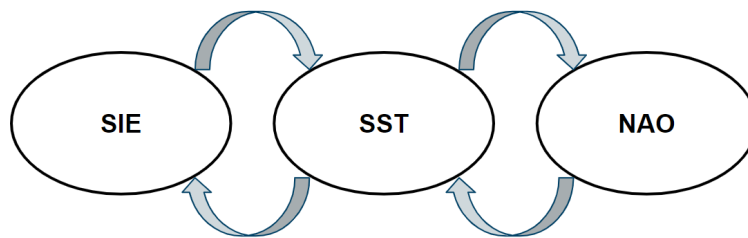


Figure 1. Schematic diagram to show the positive feedback loops among climate variables: Sea Ice Extent (SIE), Sea Surface Temperature (SST), and North Atlantic Oscillation (NAO).

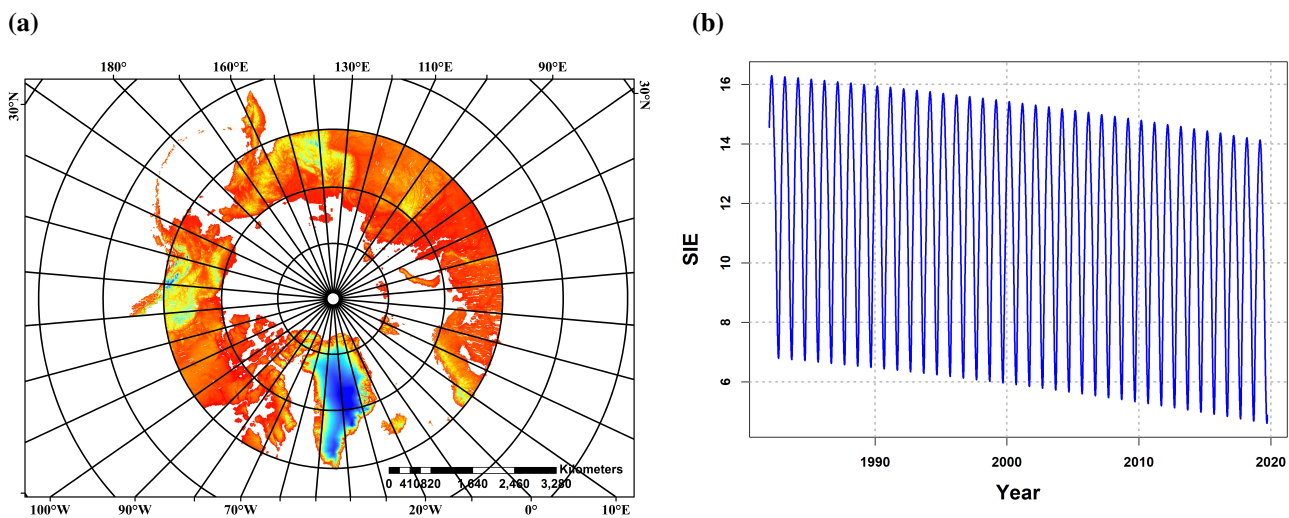


Figure 2. (a) The Digital Elevation Model of the Arctic Sea Ice region. Data sets were downloaded from <https://www.pgc.umn.edu/data/arcticdem/>, and the mapped composition was prepared using ARC GIS 1.4. (b) SIE time series plot from 1982 to 2019.

Description of data set

This study uses three different data sets: (a) daily mean Arctic SIE, (b) daily mean SST, and (c) daily mean NAO index. The NAO and SST data sets are available from the NOAA website^{34,35}. The SIE data set is available from the website of the National Snow and Ice Data Centre³⁶. The NAO data set is available from 1950, the SIE data set from 1979, and the SST

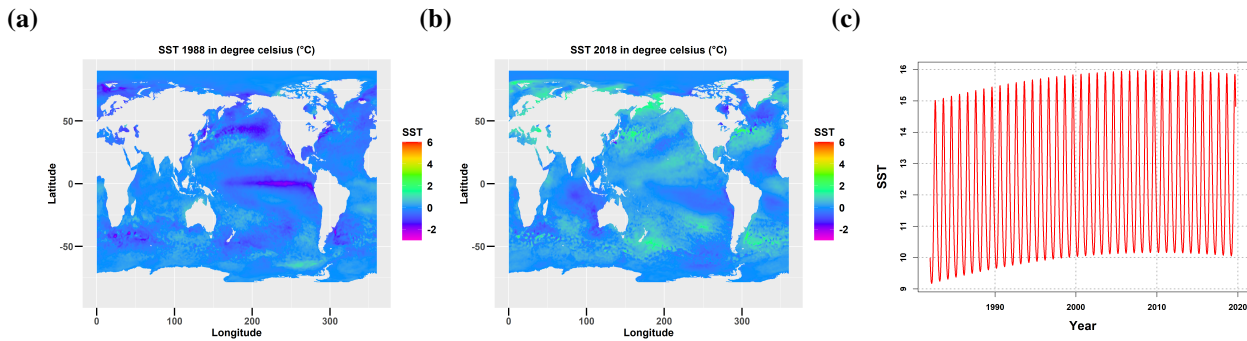


Figure 3. (a) Grid level $\delta(SST)$ for 1988 (b) Grid level $\delta(SST)$ for 2018 (c) Plot of the daily mean SST time series from 1982 to 2019.

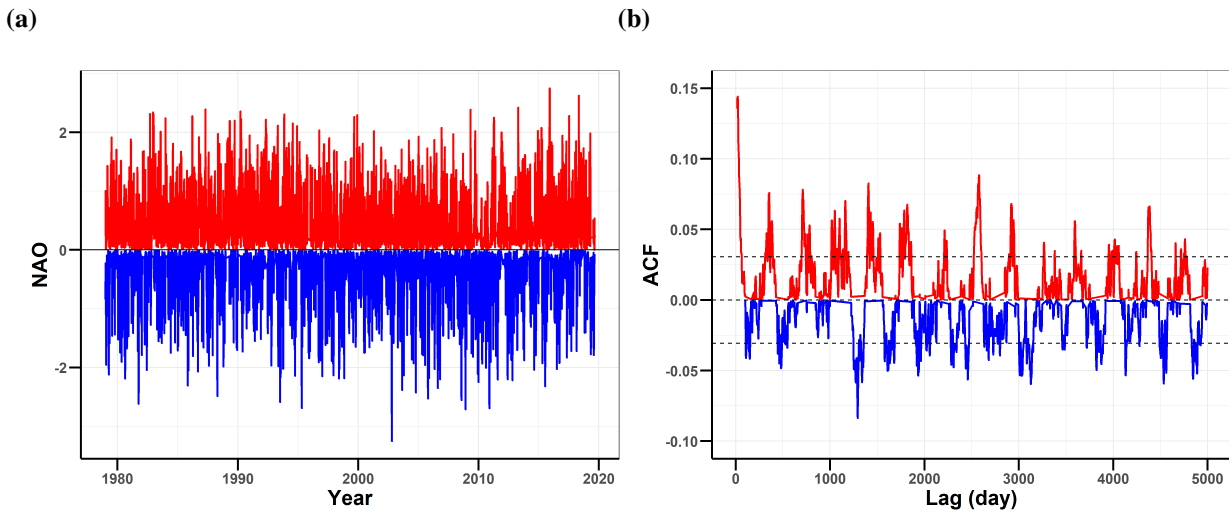


Figure 4. (a) Plot of the NAO time series over the period of 1979-2019 (b) Autocorrelation plot of NAO with a maximum lag of 5000 days (almost 13 years).

data set is available from 1982. All of these data sets are in tabular form for the entire Arctic and North Atlantic region. We considered the data from January 1982 to September 2019, extending over 38 years.

Region of Arctic Sea Ice: Arctic Circle’s position is not fixed and right now runs along 66°33 north of the equator³⁷. Subsequently, the Arctic Circle is floating northwards (shrinking) at a speed of around 15 m (49 ft) each year. The digital elevation model of the Arctic sea ice region has been shown in Figure (2a). Data sets were downloaded from <https://www.pgc.umn.edu/data/arcticdem/> and then mapped composition was prepared in ARC GIS 1.4. Figure (2b) show that the SIE is melting over time from 1982 to 2019. During the summer, the Arctic SIE decreases gradually from 7.412 square km to 3.340 square km from 1982 to 2019.

Methods and Results

Exploratory statistical analyses

Figure (3a) and (3b) presents the $\delta(SST)$ at grid level for the year 1988 and 2018, where $\delta(SST)$ at a grid level is defined as follows:

$$\delta(SST)_g = \overline{SST}_g - \widehat{SST}_g,$$

where \overline{SST}_g is the annual average of SST at grid level g , and \widehat{SST}_g is the average of all annual averages of SST at grid level g . In 1988, the $\delta(SST)$ mainly was below 0 in the majority grid levels. However, in 2018, the $\delta(SST)$ became above 2 degrees over most grids. Figure (3c) presents the overall daily mean SST (taken over all grids) from 1982 to 2019.

NAO measures the variability of air pressure at sea level between the center of the “Icelandic Low” and the center of the “Azores High”, that controls the strength and direction of westerly winds and the location of storm tracks across the North

Atlantic. Thus, the positive NAO phase would imply strong high-pressure and low-pressure systems that would create warmer and wetter conditions over northern Europe, and most of northeastern North America during winters; whereas a negative NAO would imply Eastern North America and northern Europe would have colder winters, mostly because Arctic air intrusions would occur more frequently; Europe would experience below-average precipitation, while North America would experience more snow than usual. Figure 4(a) shows that it is a mean (at zero) stationary process. It was further verified by conducting the Augmented Dickey-Fuller test, where the p-value indicates the same. Auto-correlation function (ACF) helps to find out whether the NAO has long memory or not. Plot (b) of Figure 4 presents the ACF plot of NAO with a maximum lag of 5000 days (about 13 years), indicating that NAO is a stationary process with a long memory. Table (1) presents the Hurst exponent of the NAO index, which is significantly larger than 0.5, indicating the existence of long memory in the NAO index, i.e., the path of the NAO index has a long memory, and it is mean stationary.

Methods	Hurst Exponent
Simple R/S Hurst estimation	0.73
Corrected R over S Hurst exponent	0.73
Empirical Hurst exponent	0.67
Corrected empirical Hurst exponent	0.66
Theoretical Hurst exponent	0.52

Table 1. The Hurst Exponent value of the NAO index using different methods.

Statistical Machine Learning Approach for exploring the relationship between SIE, SST, and NAO

In the statistical machine learning approach, we mainly use the Granger-causal model, which uses autoregressive time-series methods, to establish the Granger-causal relationship between the variables. We investigate the Granger-causal relations between the (a) SST and SIE and (b) SST and NAO, and vice versa.

1. Granger-causal model for SIE and SST

To test whether the changing causal dynamics of SIE vs. SST and vice versa, we present the following hypothesis using Granger Causal Model. Suppose $X(t)$ is the residual of SIE at time t , and $x(t)$ is the residual of SST at time t . The Null Hypothesis considers that SIE is a function of its historical memory only, i.e.,

Null Hypothesis (H_0):

$$X(t) = \beta_0 + \beta_1 X(t-1) + \dots + \beta_k X(t-k) + \varepsilon(t),$$

where $\varepsilon(t) \sim N(0, \sigma^2)$, is the white noise.

Alternate Hypothesis (H_a): Residual of SIE is a function of its memory and the function of residual of SST.

$$X(t) = \beta_0 + \beta_1 X(t-1) + \dots + \beta_k X(t-k) + \gamma_1 x(t-1) + \dots + \gamma_k x(t-k) + \varepsilon(t),$$

The null hypothesis says that all $\gamma_i = 0$, i.e., $H_0 : \gamma_1 = \dots = \gamma_k = 0$, to reject this in our alternate hypothesis H_a : we have to check if at least one $\gamma_i \neq 0$. The ANOVA F-test (p-value = 2.2×10^{-16}) rejects the null hypothesis, that is, more than one $\gamma_i \neq 0$. To clearly understand the effect, we consider a large number of lags by choosing $k = 365$. We implemented the LASSO feature selection³⁸ procedure to drop the lags, which have no significant effect on SIE. The rejection of the null hypothesis tells that the dynamics of SST have a significant effect on the SIE. The phase-plane analysis of SIE and SST is given in supplementary materials.

2. Granger-causal model to test the effect of SST on NAO

Null Hypothesis (H_0): NAO index is a function of only its historical memory, i.e.,

$$Y(t) = \beta_0 + \beta_1 Y(t-1) + \dots + \beta_k Y(t-k) + \varepsilon(t),$$

where $Y(t)$ is NAO index at t , and $\varepsilon(t) \sim N(0, \sigma^2)$.

Alternate Hypothesis (H_a): NAO is a function of its memory and derivatives of SST.

$$\begin{aligned} Y(t) = & \beta_0 + \beta_1 Y(t-1) + \dots + \beta_k Y(t-k) \\ & + \gamma_1 x'(t-1) + \dots + \gamma_k x'(t-k) \\ & + \alpha_1 x''(t-1) + \dots + \alpha_k x''(t-k) + \varepsilon(t), \end{aligned}$$

where $x'(t)$ is first derivative (momentum) of SST and $x''(t)$ is second derivative (acceleration) of SST.

Our next objective is to test:

$H_0 : \gamma_1 = \dots = \gamma_k = 0 = \alpha_1 = \dots = \alpha_k = 0$ vs. H_a : at least one γ_i or $\alpha_i \neq 0$. The ANOVA F-test (p-value = 0.00206) rejects the null hypothesis, at least one $\gamma_i, \alpha_i \neq 0$. To clearly understand the effect, we consider a large number of lags by choosing $k = 365$. By implementing the LASSO selection,³⁸ procedure, we drop the lags, which have no significant effect on NAO. The rejection of the null hypothesis indicates that the dynamics of SST have a significant effect on the NAO index, considering the long memory of NAO in the model.

3. Granger-causal model to test the effect of NAO on SST

Null Hypothesis (H_0): Suppose $Y(t)$ is the first derivative(momentum) of SST at time t , which is a function of its historical memory only, i.e.,

$$Y(t) = \beta_0 + \beta_1 Y(t-1) + \dots + \beta_k Y(t-k) + \varepsilon(t),$$

where $Y(t)$ is first derivative of SST at t , and $\varepsilon(t) \sim N(0, \sigma^2)$.

Alternate Hypothesis (H_a): The first derivative of SST is a function of its historical memory and the NAO index, i.e.,

$$\begin{aligned} Y(t) = & \beta_0 + \beta_1 Y(t-1) + \dots + \beta_k Y(t-k) \\ & + \alpha_1 x(t-1) + \dots + \alpha_k x(t-k) + \varepsilon(t), \end{aligned}$$

where $Y(t)$ is momentum or first derivative of SST, and $x(t)$ is the NAO index. Our final objective is to test:

$H_0 : \alpha_1 = \dots = \alpha_k = 0$ vs. H_a : at least one $\alpha_i \neq 0$.

The p-value = 0.00356 for ANOVA F-test indicates rejection of the null model. It means the long memory of NAO has a statistically significant effect on the momentum of SST. A similar analysis was carried out with the second derivative of SST. It was found that the long memory of NAO also has a statistically significant effect on the second derivative of SST.

4. Bayesian Granger-causal dynamic linear model (BGDLM)

Kolstad *et al.*²⁸ had criticized the statistical models for climate research, citing the reason that the relationship between the predictor and dependent variable did not change over time (i.e., regression coefficients remained constant over time). Here, we take into account this criticism by constructing a BGDLM, along the line of the work by Das *et al.*³³, where the relationship between a predictor and the dependent variable is updated over over time by updating the coefficients, as follows:

$$y_t = \beta_{0t} + \beta_{1t} y_{t-1} + \gamma_{1t} x_{t-1} + \varepsilon_t, \quad (1)$$

$$\beta_{0t} = \rho_0 \beta_{0,t-1} + \eta_{1t}, \quad (2)$$

$$\beta_{1t} = \rho_1 \beta_{1,t-1} + \eta_{2t}, \quad (3)$$

$$\gamma_{1t} = \rho_2 \gamma_{1,t-1} + \eta_{3t}, \quad (4)$$

where Equation (1) is known as observation equation; and Equation (2, 3,4) are known as the system equations; the y_t is NAO at time point t ; the x_t is the momentum of SIE at time point t ; ε_t is white noise follows $N(0, \sigma_\varepsilon^2)$; η_{jt} , $j = 1, 2, 3$ are white noise associated with system equation follows $N(0, \sigma_{\eta_j}^2)$. Note that $\rho = (\rho_0, \rho_1, \rho_2)$ should be bounded, that is, $|\rho_j| < 1$, such that the model would be a stationary process like the NAO index. We know that NAO is a mean stationary process; see Figure 4(a); hence this restriction of ρ_j is required. We present the Equation (1) and Equation (2,3,4) in the matrix notations as follows:

$$\begin{aligned} Y_t &= X_t \beta_t + \varepsilon_t, \quad \text{observation equation,} \\ \beta_t &= R \beta_{t-1} + \eta_t, \quad \text{system equation,} \end{aligned} \quad (5)$$

where $\varepsilon_t \sim N(0, \sigma^2)$, and $\eta_t \sim N(0, Q)$. The Bayesian update solution (aka., Kalman filter) for Equation (5) can be taken from^{33,39}, as follows

$$\begin{aligned} K_t &= R\Sigma_t X_t^T (X_t \Sigma_t X_t^T + \sigma^2)^{-1}, \\ \hat{\beta}_{t+1} &= R\hat{\beta}_t + K_t(Y_t - X_t \hat{\beta}_t), \\ \Sigma_{t+1} &= R\Sigma_t R^T - K_t X_t \Sigma_t R^T + Q. \end{aligned} \quad (6)$$

In this study, BGDLM corresponds to the Equation (9) developed. These models are then updated by the BGDLM using a Kalman filter, as presented in Equation (6). Through these Kalman updates, β coefficients are dynamically updated. The model for SIE is as follows:

$$y(t) = \beta_0(t) + \beta_1(t) \sin(\omega t) + \gamma_1(t) \cos(\omega t) + \varepsilon, \quad (7)$$

where $y(t)$ is SIE extent at time point t ; $\beta_0(t)$, $\beta_1(t)$ and $\gamma_1(t)$ are the dynamic coefficients, updated via Kalman update Equation (6). Note that the model does not have any trend part because if there is any trend in the data, that will be captured automatically in the coefficients. In addition, the BGDLM was built in the following way:

$$y(t) = \beta_0(t) + \sum_{k=1}^K \beta_k(t)y(t-1) + \sum_{k=1}^K \gamma_k(t)x(t-k) + \varepsilon(t), \quad (8)$$

where $y(t)$ is NAO and $x(t-k)$ is the momentum of the SIE at $(t-k)$. Here, the Akaike information criterion type model selection process was used to obtain the optimal choice for the Model Equation (8). It may be noted that if the model's coefficients are static, then the Granger causal model is a special case of Equation (8).

	ρ	CI	p-value	Skewness of NAO
Daily	-0.20	[-0.22,-0.18]	$2.2 * 10^{-16}$	-0.21
Monthly	-0.30	[-0.38,-0.21]	$8.4 * 10^{-11}$	-0.19
Yearly	-0.60	[-0.79,-0.31]	0.00038	-0.46

Table 2. Chart of values for (i) correlation coefficient (ρ), along with the confidence interval (CI), and p-value between NAO and SST on a daily, monthly, and yearly scales. (ii) Corresponding skewness of NAO.

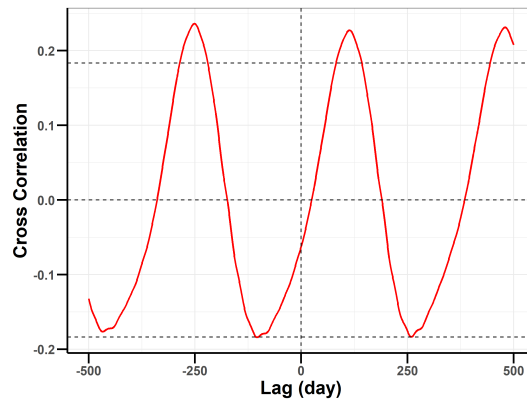


Figure 5. Plot of cross-correlation function between NAO and the first derivative of lagged values of SST.

Summary and Discussions

In summary, we have studied the complex dynamics and critical instability (through positive feedback loops) among the three climate variables of the melting SIE, rising SST, and NAO, using a generic approach of statistical machine learning. This approach is less computationally intensive and more general than the sophisticated climate forecast models, allowing us to perform our analyses over the entire North Atlantic region. Also, through our Bayesian Granger-causal dynamic linear model, we were able to address the major criticism of the statistical models by Kolstad²⁸.

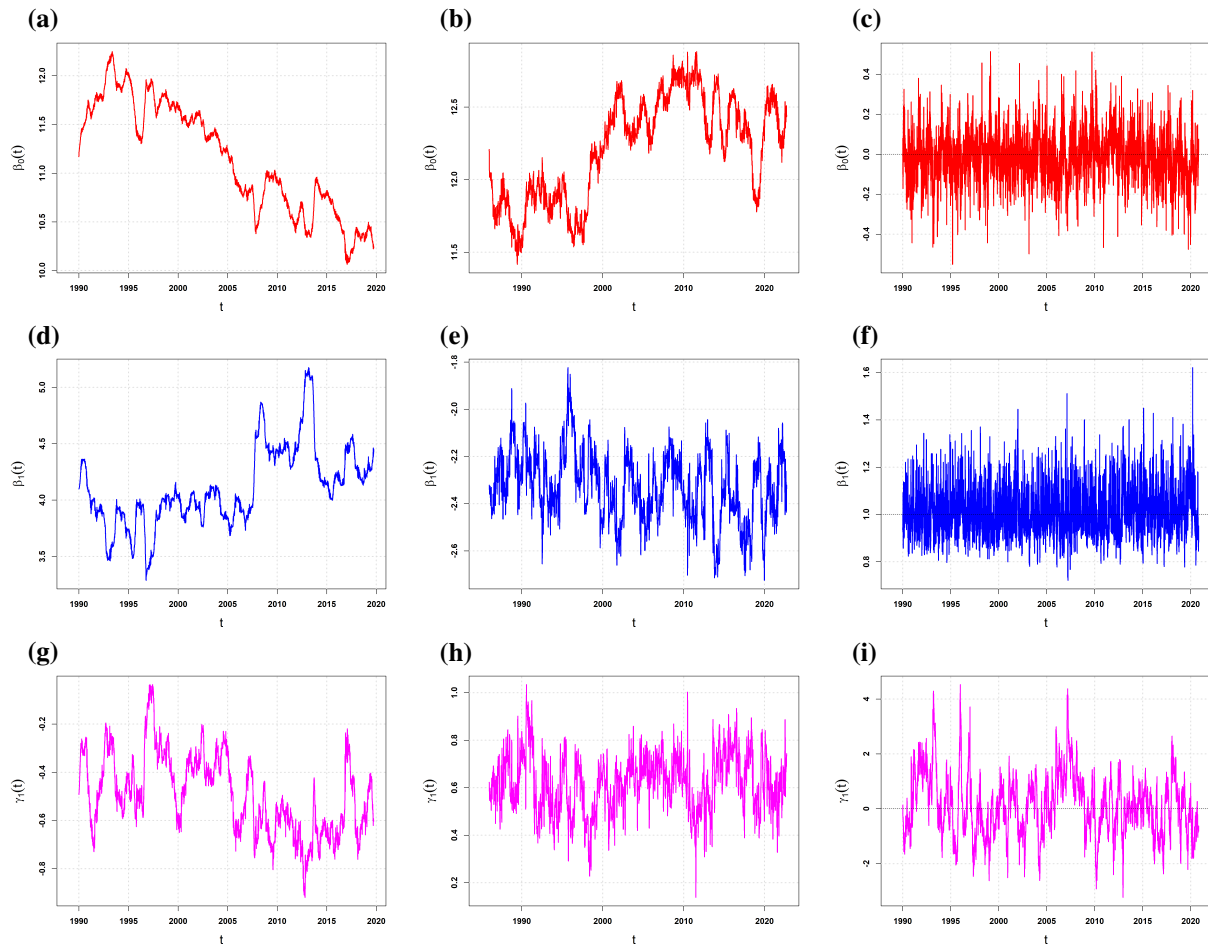


Figure 6. (a) The downward trend in the dynamic intercept $\beta_0(t)$ of SIE indicates that the SIE is shrinking over time. (b) The downward trend in the dynamic intercept $\beta_0(t)$ of SST indicates increasing trend in SST. (c) The dynamic intercept $\beta_0(t)$ of NAO is mean-zero stationary process like $NAO(t)$. (d) The dynamic coefficient $\beta_1(t)$ corresponding to $\sin \omega t$ for $SIE(t)$. (e) The dynamic coefficient $\beta_1(t)$ corresponding to $\sin \omega t$ for $SST(t)$. (f) The dynamic coefficient $\beta_1(t)$ corresponding to $NAO(t-1)$ for $NAO(t)$. (g) The dynamic coefficient $\gamma_1(t)$ corresponding to $\cos \omega t$ for $SIE(t)$. (h) The dynamic coefficient $\gamma_1(t)$ corresponding to $\cos \omega t$ for $SST(t)$. (i) The dynamic coefficient $\gamma_1(t)$ corresponding to $SST(t)$ for $NAO(t)$.

Our major findings were: (i) SIE and SST Granger causes each other; (ii) SST and NAO also Granger causes each other; (iii) SST and NAO are anti-correlated, which implies that increasing trend of SST would lead to more frequent occurrences of negative NAO. This is corroborated by the fact that the skewness of NAO index is negative (at different time scales – daily, monthly and yearly) as listed in Table (2). Very interestingly, though NAO itself is a mean-zero stationary process (as shown in Figure(4:a), a negative skewness of NAO would mean that a negative NAO is more likely to occur than a positive NAO, resulting in critical instability in the climate system of the North Atlantic region, especially in northern Europe and the North American region. We would thus expect that there would be more frequent bouts of very cold climate in eastern North America and northern Europe than previously seen, marking a significant climate change. Overall this study is an essential contribution toward understanding the critical instability of complex climate systems using statistical machine learning-based techniques.

References

1. Halloran, P. *et al.* Natural drivers of multidecadal arctic sea ice variability over the last millennium. *Sci. Reports* **10**, 688, DOI: [10.1038/s41598-020-57472-2](https://doi.org/10.1038/s41598-020-57472-2) (2020).
2. Lindsey, R. & Dahlman, L. Climate variability: North atlantic oscillation (2009). NOAA:Climate.gov <https://www.climate.gov/news-features/understanding-climate/climate-variability-north-atlantic-oscillation>.

3. Dall’Osto, M. *et al.* Arctic sea ice melt leads to atmospheric new particle formation. *Sci. Reports* **7**, 3318, DOI: [10.1038/s41598-017-03328-1](https://doi.org/10.1038/s41598-017-03328-1) (2017).
4. Jaiser, R., Dethloff, K., Handorf, D., Rinke, A. & Cohen, J. Impact of sea ice cover changes on the northern hemisphere atmospheric winter circulation. *Tellus A: Dyn. Meteorol. Oceanogr.* **64**, 11595, DOI: [10.3402/tellusa.v64i0.11595](https://doi.org/10.3402/tellusa.v64i0.11595) (2012). <https://doi.org/10.3402/tellusa.v64i0.11595>.
5. Dai, G., Mu, M. & Wang, L. The influence of sudden arctic sea-ice thinning on north atlantic oscillation events. *Atmosphere-Ocean* **59**, 39–52, DOI: [10.1080/07055900.2021.1875976](https://doi.org/10.1080/07055900.2021.1875976) (2021). <https://doi.org/10.1080/07055900.2021.1875976>.
6. Horvath, S., Stroeve, J., Rajagopalan, B. & Jahn, A. Arctic sea ice melt onset favored by an atmospheric pressure pattern reminiscent of the north american- Eurasian arctic pattern. *Clim. Dyn.* **57**, DOI: [10.1007/s00382-021-05776-y](https://doi.org/10.1007/s00382-021-05776-y) (2021).
7. Das, P., Lahiri, A. & Das, S. Understanding sea ice melting via functional data analysis. *Curr. Sci.* **115**, 920–929 (2018).
8. Cressey, D. Arctic sea ice at record low. *Nature* DOI: [10.1038/news070917-3](https://doi.org/10.1038/news070917-3) (2007).
9. Delworth, T. L. *et al.* The North Atlantic Oscillation as a driver of rapid climate change in the Northern Hemisphere. *Nat. Geosci.* **9**, 509–512, DOI: [10.1038/ngeo2738](https://doi.org/10.1038/ngeo2738) (2016).
10. Castro-Díez, Y., Pozo-Vázquez, D., Rodrigo, F. S. & Esteban-Parra, M. J. Nao and winter temperature variability in southern Europe. *Geophys. Res. Lett.* **29**, 1–1–1–4, DOI: <https://doi.org/10.1029/2001GL014042> (2002). <https://agupubs.onlinelibrary.wiley.com/doi/pdf/10.1029/2001GL014042>.
11. Warner, J. L. Arctic sea ice – a driver of the winter nao? *Weather* **73**, 307–310, DOI: <https://doi.org/10.1002/wea.3399> (2018). <https://rmets.onlinelibrary.wiley.com/doi/pdf/10.1002/wea.3399>.
12. Becker, G. A. & Pauly, M. Sea surface temperature changes in the north sea and their causes. *ICES J. Mar. Sci.* **53**, 887–898, DOI: [10.1006/jmsc.1996.0111](https://doi.org/10.1006/jmsc.1996.0111) (1996). <https://academic.oup.com/icesjms/article-pdf/53/6/887/1597685/53-6-887.pdf>.
13. Cook, B. I., Mann, M. E., D’Odorico, P. & Smith, T. M. Statistical simulation of the influence of the nao on European winter surface temperatures: Applications to phenological modeling. *J. Geophys. Res. Atmospheres* **109**, DOI: <https://doi.org/10.1029/2003JD004305> (2004). <https://agupubs.onlinelibrary.wiley.com/doi/pdf/10.1029/2003JD004305>.
14. Pan, L.-L. Observed positive feedback between the nao and the north atlantic ssta tripole. *Geophys. Res. Lett.* **32**, DOI: <https://doi.org/10.1029/2005GL022427> (2005). <https://agupubs.onlinelibrary.wiley.com/doi/pdf/10.1029/2005GL022427>.
15. Slonosky, V. C. & Yiou, P. The north atlantic oscillation and its relationship with near surface temperature. *Geophys. Res. Lett.* **28**, 807–810, DOI: <https://doi.org/10.1029/2000GL012063> (2001). <https://agupubs.onlinelibrary.wiley.com/doi/pdf/10.1029/2000GL012063>.
16. Max, L. *et al.* Sea surface temperature variability and sea-ice extent in the subarctic northwest Pacific during the past 15,000 years. *Paleoceanography* **27**, DOI: <https://doi.org/10.1029/2012PA002292> (2012). <https://agupubs.onlinelibrary.wiley.com/doi/pdf/10.1029/2012PA002292>.
17. Xu, H., Kim, H.-M., Nye, J. A. & Hameed, S. Impacts of the north atlantic oscillation on sea surface temperature on the northeast US continental shelf. *Cont. Shelf Res.* **105**, 60–66, DOI: <https://doi.org/10.1016/j.csr.2015.06.005> (2015).
18. Lim, Y.-K., Cullather, R. I., Nowicki, S. M. J. & Kim, K.-M. Inter-relationship between subtropical Pacific sea surface temperature, arctic sea ice concentration, and north atlantic oscillation in recent summers. *Sci. Reports* **9**, 3481, DOI: [10.1038/s41598-019-39896-7](https://doi.org/10.1038/s41598-019-39896-7) (2019).
19. Hurrell, J. W. & Deser, C. North atlantic climate variability: The role of the north atlantic oscillation. *J. Mar. Syst.* **78**, 28–41, DOI: <https://doi.org/10.1016/j.jmarsys.2008.11.026> (2009).
20. Kwok, R. Recent changes in arctic ocean sea ice motion associated with the north atlantic oscillation. *Geophys. Res. Lett.* **27**, 775–778, DOI: <https://doi.org/10.1029/1999GL002382> (2000). <https://agupubs.onlinelibrary.wiley.com/doi/pdf/10.1029/1999GL002382>.
21. Miettinen, A., Koç, N., Hall, I. R., Godtliebsen, F. & Divine, D. North atlantic sea surface temperatures and their relation to the north atlantic oscillation during the last 230 years. *Clim. Dyn.* **36**, 533–543, DOI: [10.1007/s00382-010-0791-5](https://doi.org/10.1007/s00382-010-0791-5) (2011).
22. Parkinson, L. C. Recent trend reversals in arctic sea ice extents: Possible connections to the north atlantic oscillation. *Polar Geogr.* **24**, 1–12, DOI: [10.1080/10889370009377684](https://doi.org/10.1080/10889370009377684) (2000). <https://doi.org/10.1080/10889370009377684>.
23. Koslowski, G. & Loewe, P. The western baltic sea ice season in terms of a mass-related severity index: 1879–1992. *Tellus A: Dyn. Meteorol. Oceanogr.* **46**, 66–74, DOI: [10.3402/tellusa.v46i1.15433](https://doi.org/10.3402/tellusa.v46i1.15433) (1994). <https://doi.org/10.3402/tellusa.v46i1.15433>.

24. Kvamstø, N. G., Skeie, P. & Stephenson, D. B. Impact of labrador sea-ice extent on the north atlantic oscillation. *Int. J. Climatol.* **24**, 603–612, DOI: <https://doi.org/10.1002/joc.1015> (2004). <https://rmets.onlinelibrary.wiley.com/doi/pdf/10.1002/joc.1015>.
25. Bader, J. *et al.* A review on northern hemisphere sea-ice, storminess and the north atlantic oscillation: Observations and projected changes. *Atmospheric Res.* **101**, 809–834, DOI: <https://doi.org/10.1016/j.atmosres.2011.04.007> (2011).
26. Caian, M., Koenigk, T., Döscher, R. & Devasthale, A. An interannual link between arctic sea-ice cover and the north atlantic oscillation. *Clim. Dyn.* **50**, 423–441, DOI: [10.1007/s00382-017-3618-9](https://doi.org/10.1007/s00382-017-3618-9) (2018).
27. Tian, B. & Fan, K. A skillful prediction model for winter nao based on atlantic sea surface temperature and eurasian snow cover. *Weather. Forecast.* **30**, 197 – 205, DOI: [10.1175/WAF-D-14-00100.1](https://doi.org/10.1175/WAF-D-14-00100.1) (2015).
28. Kolstad, E. W. & Screen, J. A. Nonstationary relationship between autumn arctic sea ice and the winter north atlantic oscillation. *Geophys. Res. Lett.* **46**, 7583–7591, DOI: <https://doi.org/10.1029/2019GL083059> (2019). <https://agupubs.onlinelibrary.wiley.com/doi/pdf/10.1029/2019GL083059>.
29. Kennel, C. F. & Yulaeva, E. Influence of arctic sea-ice variability on pacific trade winds. *Proc. Natl. Acad. Sci.* **117**, 2824–2834, DOI: [10.1073/pnas.1717707117](https://doi.org/10.1073/pnas.1717707117) (2020). <https://www.pnas.org/doi/pdf/10.1073/pnas.1717707117>.
30. Riaz, S. M. F., Iqbal, M. J. & Hameed, S. Impact of the north atlantic oscillation on winter climate of germany. *Tellus A: Dyn. Meteorol. Oceanogr.* **69**, 1406263, DOI: [10.1080/16000870.2017.1406263](https://doi.org/10.1080/16000870.2017.1406263) (2017). <https://doi.org/10.1080/16000870.2017.1406263>.
31. Petris, G., Petrone, S. & Campagnoli, P. *Dynamic Linear Models with R*, vol. 38, 31–84 (Springer New York, NY, 2009).
32. Migon, H. S., Petris, S., G. and Petrone & Campagnoli, P. Dynamic linear models with R. *Biometrics* **66**, 1311–1312, DOI: <https://doi.org/10.1111/j.1541-0420.2010.01512.x> (2010). <https://onlinelibrary.wiley.com/doi/pdf/10.1111/j.1541-0420.2010.01512.x>.
33. Das, S. & Dey, D. K. On dynamic generalized linear models with applications. *Methodol. Comput. Appl. Probab.* **15**, 407–421, DOI: [10.1007/s11009-011-9255-6](https://doi.org/10.1007/s11009-011-9255-6) (2013).
34. NSIDC. Daily sea ice extent. Data can be downloaded from: <https://psl.noaa.gov/repository/entry/show?entryid=f8d470f4-a072-4c1e-809e-d6116a393818>.
35. NOAA. Noaa optimum interpolation (oi) sea surface temperature (sst) v2. Data can be downloaded from: <https://psl.noaa.gov/repository/entry/show?entryid=f8d470f4-a072-4c1e-809e-d6116a393818>.
36. NOAA. Daily nao index since january 1950. Data can be downloaded from: <https://nsidc.org/data/G02135/versions/3>.
37. Tannerr, J. Obliquity of the ecliptic, nutation in obliquity and latitudes of the arctic/antarctic circles. PHP Science Labs http://www.neoprogrammics.com/obliquity_of_the_ecliptic/.
38. Tibshirani, R. Regression shrinkage and selection via the lasso. *J. Royal Stat. Soc. Ser. B (Methodological)* **58**, 267–288 (1996).
39. Meinhold, R. J. & Singpurwalla, N. D. Understanding the kalman filter. *The Am. Stat.* **37**, 123–127, DOI: [10.1080/00031305.1983.10482723](https://doi.org/10.1080/00031305.1983.10482723) (1983). <https://www.tandfonline.com/doi/pdf/10.1080/00031305.1983.10482723>.

Acknowledgements

A.Y. is grateful for the fellowship from JNU and hospitality at CMI funded by AlgoLabs. S.D. acknowledges the partial financial support from Infosys Foundation, TATA Trust, and Bill & Melinda Gates Foundation’s grant to CMI.

Author contributions

A.C., S.D., and A.Y. conceived the research, S.D. and A.Y. developed the methods, S.D. contributed to the methods with results, and A.Y. and K.S. analyzed the results and prepared the figures. All authors discussed the results, contributed to the writing of the manuscript, and reviewed the manuscript.

Ethics declarations

Competing interests: The authors declare no competing interests.

Additional information

Time Series and Lead-Lag Cross Correlation Plots

We consider the yearly average value of both NAO and SST. We see that NAO and SST are anti-correlated to each other and the Pearson's product-moment correlation is -0.597, and 95% confidence interval is (-0.785, -0.308) with p-value = 0.000388. Figure(7) presents the lead-lag correlations plot.

Phase-plane analysis of SIE and SST

Suppose $x(t)$ is the SIE at time point t . We modeled SIE as the function of a trend and seasonal component in the following way. Trend defines long-term increase or decrease. Seasonality defines reoccurring pattern at a fixed and known frequency based on a time of the year, week, or day,

$$x(t) = \underbrace{\beta_0 + \beta_1 t + \beta_2 t^2}_{\text{trend}} + \underbrace{\left\{ \sum_{i=1}^K \beta_i \sin(i\omega t) + \sum_{i=1}^K \gamma_i \cos(i\omega t) \right\}}_{\text{seasonality}} + \varepsilon(t), \quad (9)$$

where ε is white noise with $\mathbb{E}(\varepsilon) = 0$, and $\text{Var}(\varepsilon) = \sigma^2$. In seasonality component, we consider the periodicity with $\omega = \frac{2\pi}{365}$; β_i is the coefficient corresponding to sine of i^{th} harmonics and γ_i is the coefficient corresponding to the cosine of the i^{th} harmonics. In the model, we consider K harmonics for each period. The first derivative (momentum) and second derivative (acceleration) of the model presented in the above Equation (9) are:

$$x'(t) = \underbrace{\beta_1 + 2\beta_2 t}_{\text{trend}} + \omega i \underbrace{\left\{ \sum_{i=1}^K \beta_i \cos(i\omega t) - \sum_{i=1}^K \gamma_i \sin(i\omega t) \right\}}_{\text{seasonality}} + \varepsilon_1(t) \quad (10)$$

$$x''(t) = \underbrace{2\beta_2}_{\text{trend}} + \omega^2 \underbrace{\left\{ \sum_{i=1}^K \beta_i \sin(i\omega t) + \sum_{i=1}^K \gamma_i \cos(i\omega t) \right\}}_{\text{seasonality}} + \varepsilon_2(t), \quad (11)$$

where ε_1 and ε_2 are white noise corresponding to momentum and acceleration signal.

In Figure 8(a,b), the phase-plane analysis of SIE, we see that there are major changes in area and rate of change in volume of SIE. The area of the phase plane for 2018 is more than that of 1988. Figures show that the phase-line distribution is varying, i.e., the area under the two curves is increasing, and the rate at which sea ice is melting is also comparatively increasing from 1988 to 2018, and that is happening due to the melting SIE. Figure (9) presents the forecasted and actual path in the test dataset from 2010 to 2019. Root Mean Square Error (RMSE) was calculated for training and test datasets. For the training sample, the value of RMSE is 0.36, and for the test dataset, the value of RMSE is 0.41. The value of R-squared is 0.9865, which indicates the model generalises very well in the out of sample.

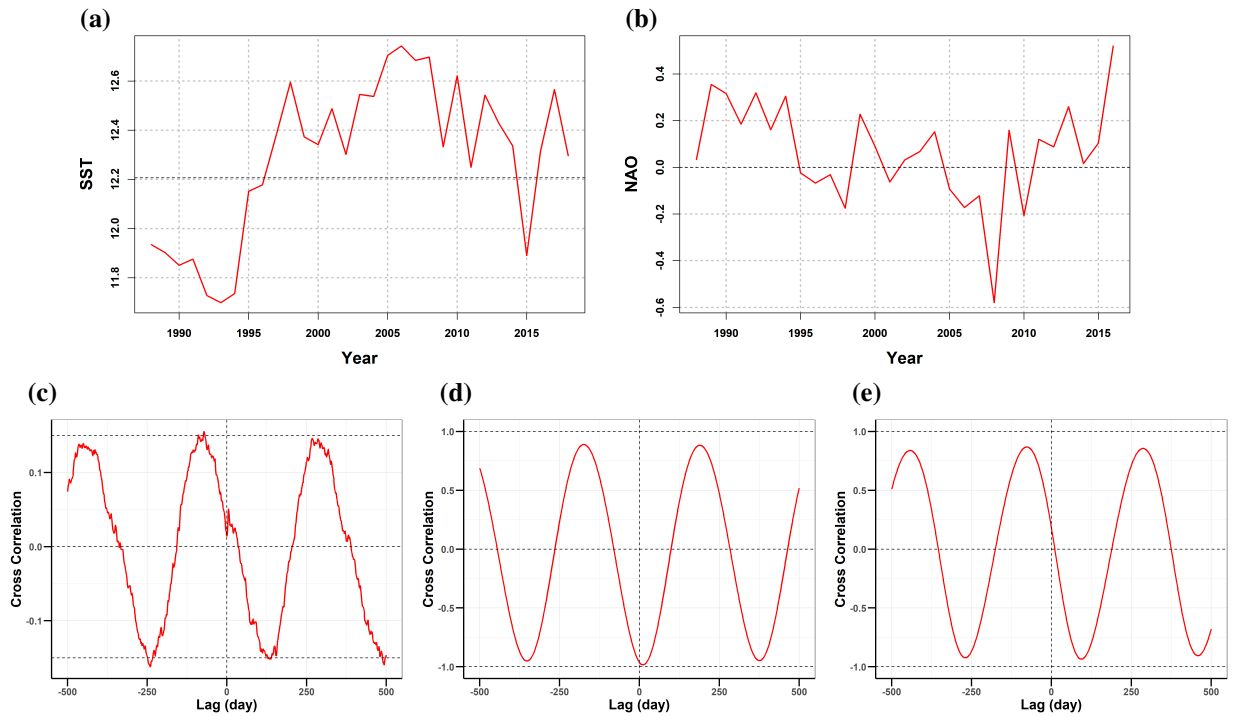


Figure 7. (a) Plot of annual average SST for the considered period from 1988 to 2018. (b) Plot of annual average NAO for the considered period from 1988 to 2018. (c) Plot of cross-correlation between NAO and the first derivative of lagged values of SIE. (d) Plot represents the cross-correlation between SIE and SST. (e) Plot represents the cross-correlation between SIE and the first derivative of SST. For all lagged cross correlation, we considered the lag values of 500 days.

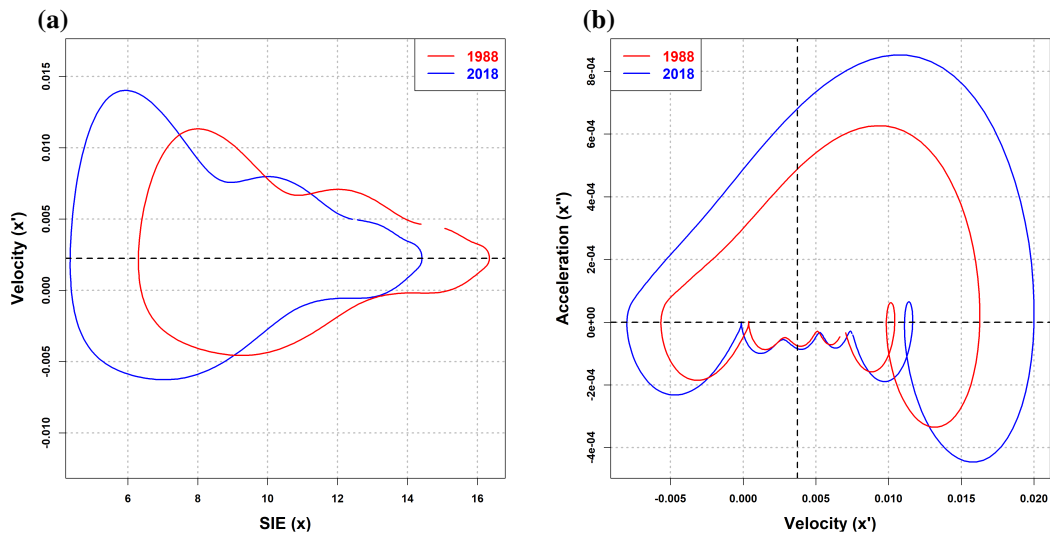


Figure 8. (a) Phase-line plot of SIE $x(t)$ as per Equation (9) vs. velocity of SIE $x'(t)$ as per Equation (10) for the two years 1988 and 2018. (b) Phase-plane plot of velocity of SIE $x'(t)$ as per Equation (10) vs. acceleration of SIE $x''(t)$ as per Equation (11) for the two years 1988 and 2018.

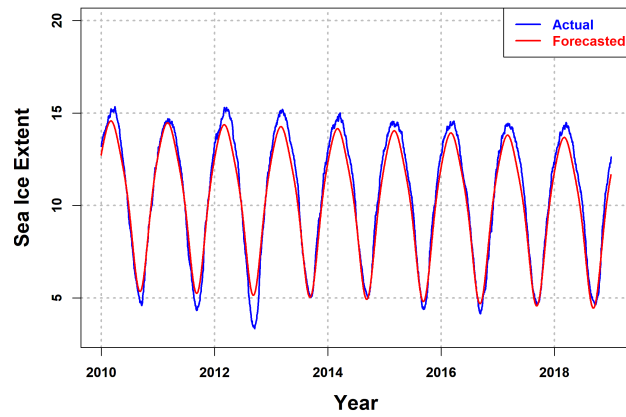


Figure 9. To test the performance of our proposed model (Equations (9,10,11)), we conducted a machine learning test. We considered the training data set from 1979 to 2009 and the test data from 2010 to 2019.